

# The research on small-scale structures of ice particle density and electron density in the mesopause region

Ruihuan Tian<sup>1,2</sup>, Jian Wu<sup>2</sup>, Jinxiu Ma<sup>3</sup>, Yonggan Liang<sup>1,2</sup>, Hui Li<sup>1,2</sup>, Chengxun Yuan<sup>1,4</sup>, Yongyuan Jiang<sup>1</sup> and Zhongxiang Zhou<sup>1,4</sup>

<sup>1</sup>Department of Physics, Harbin Institute of Technology, Harbin 150001, China

<sup>2</sup>National Key Laboratory of Electromagnetic Environment (LEME), China Research Institute of Radio Wave Propagation, Beijing 102206, China

<sup>3</sup>CAS Key Laboratory of Geospace Environment and Department of Modern Physics, University of Science and Technology of China, Hefei 230026, China

<sup>4</sup>Center of Space Environment of Polar Regions, Harbin Institute of Technology, Harbin 150001, China

Correspondence to: Chengxun Yuan ([yuancx@hit.edu.cn](mailto:yuancx@hit.edu.cn)) and Hui Li ([lihui\\_2253@163.com](mailto:lihui_2253@163.com))

**Abstract.** A growth and motion model is developed to give a possible explanation on the formation of ice particle density irregularities with meter scale, which are the major players in the generation and persistence of small scale electron density fluctuations that can cause polar mesosphere summer echoes (PMSE) phenomenon. The evolution of radius, velocity, and number density of ice particles in mesopause region is investigated based on the growth and motion model. In the growth model, meteoric dust from outer atmosphere and grains moving upward with the neutral wind from the mesosphere bottom serve as nuclei upon which water vapor can condense in the cold and moist condition. And the motion of the ice particles is mainly controlled by gravity and the neutral drag force. It is shown that, for certain nucleus radius, the velocity of particles can be reversed at particular height, which leads to local gathering of particles near the boundary layer and stable small-scale ice particle density structures. Then the influence of these stable small-scale structures on electron and ion density is studied by a charging model, which considers the production, loss and transport of electrons and ions, and dynamic particle charging processes. The results show that, for particles with radii of 11 nm or less, the electron density is anti-correlated to charged ice particle density and ion density due to plasma attachment by particles and plasma diffusion, which is in accordance with most rocket observations.

## 1 Introduction

The polar mesosphere summer echoes (PMSE) are strong radar echoes from the polar mesopause in

summer(Rapp and Lübken 2004). One of the features of PMSE is that the spectra widths of echoes are  
30 much narrower than that of incoherent scatter (being due to the Brownian movement of  
electrons)(Röttger, et al. 1988;Röttger, et al. 1990). And it has been proposed that the PMSEs are radar  
waves coherently scattered by the irregularities of the refractive index which are mainly determined by  
electron density(Rapp and Lübken 2004). Furthermore, the efficient scattering occurs when the spatial  
scale of electron density structures is half of the radar wavelength, the so-called Bragg scale. For typical  
35 VHF radars, the scale is about 3 m(Rapp and Lübken 2004). Experimentally, in the ECT02  
campaign(Lübken, et al. 1998), the sounding rocket with electron probe has detected electron density  
irregularities on the order of meters during the simultaneous observation of PMSE, which provides a  
vital argument for that small-scale electron density structures can indeed create strong radar echoes.

Lots of researches indicate that small scale ice particle density irregularities in the PMSE region play  
40 a key role in creating and maintaining small-scale structures of electron density (Chen and Scales  
2005;Lie - Svendsen, et al. 2003;Mahmoudian and Scales 2013;Rapp and Lübken 2003;Scales and  
Ganguli 2004). Markus Rapp and Franz-Josef Lübken investigated electron diffusion in the vicinity of  
charged particles revisited (Rapp and Lübken 2003). They developed coupled diffusion equations for  
45 electrons, charged aerosol particles, and positive ions subject to the initial condition of anti-correlated  
perturbations in the charged aerosol and electron distribution. These solutions showed that electron  
perturbations were anti-correlated to both perturbations in the distributions of negatively charged  
aerosol particles and positive ions. And the lifetime of these perturbations was determined by aerosol  
particle diffusion. For particles with radii larger than  $\sim 10$  nm, electron number density perturbations  
could maintain for several hours after the initial creation mechanism of particle density perturbations  
50 stopped. Ø. Lie-Svendsen et al studied the response of the mesopause plasma to small-scale aerosol  
particle density perturbations based on time-dependent, one-dimensional, coupled continuity and  
momentum equations for an arbitrary number of charged and neutral particle species (Lie - Svendsen, et  
al. 2003). The results were consistent with the solution of Markus Rapp's model that particle density  
structures on the order of a few meters could lead to small-scale electron density perturbations due to  
55 electron attachment and ambipolar diffusion.

In all researches mentioned above, the aerosol particle density profiles were directly set as specific  
small scale structures such as Gaussian, hyperbolic tangent or sinusoidal. And the formation processes

of these small-scale particle density structures have always been neglected, though they are helpful to understand PMSE phenomenon better. In view of this, the purpose of this study is trying to explain the formation of these ice particle irregularities through a growth and motion model. The growth of particles is based on collision and adsorption process of water vapor and condensation nuclei. The particle movement is mainly controlled by the gravity and the neutral drag force. With the obtained ice particle density structures, the corresponding electron and ion density is calculated based on a charging model, in which the dynamic continuity equations for ice particles with various charges and ions, momentum equation for ions and electrons, and quasi-neutral condition are included.

## 2 Model

In this section the equations of the growth and motion model of condensation nuclei and the charging model of ice particles are described.

The simulation is carried out at summer polar mesopause region between 80 ~ 90 km, where the water vapor carried by neutral gas is supposed to move upwards at a constant speed(Garcia and Solomon 1985). It is assumed that micrometeorites enter the study region at a certain flux from the upper boundary, and volcanic ash or particles ejected by aircraft rise into the region from the lower boundary. These grains serve as condensation cores. With the temperature lower than the frost point(Körner and Sonnemann 2001), the water vapor molecules that touch the surface of the grains due to thermal motion can easily condense into ice, which makes condensation cores become ice particles and keep growing. In this article, we will only discuss the growth, motion and charging of particles inside the condensation layer. Meantime, only vertical transport of particles and plasma is considered in this paper, because the horizontal gradients of transport parameters are much smaller than the vertical ones(Lie - Svendsen, et al. 2003).

For growing ice particles, the dynamic equation for variable mass object is applied:

$$m_d \frac{d\mathbf{u}_d}{dt} + (\mathbf{u}_d - \mathbf{u}) \frac{dm_d}{dt} = m_d \mathbf{g} - \mu_{dn} m_d (\mathbf{u}_d - \mathbf{u}) + q_d \mathbf{E} \quad (1)$$

where  $m_d$ ,  $\mathbf{u}_d$  and  $q_d$  are the mass, velocity, and charge of ice particles respectively.  $\mathbf{u}$  is the velocity of neutral gas;  $\mathbf{g}$  is the gravitational acceleration;  $\mu_{dn}$  is the collision frequency between ice particles and gas; and  $\mathbf{E}$  is the electric field. The electric force has trivial effect on the motion of ice particles, because the charge-mass ratio of particles is usually very small(Jensen and Thomas 1988;Pfaff, et al. 2001). The

inertial term is also negligible since its magnitude is much smaller than gravity (Garcia and Solomon 1985).

We assume that all water molecules colliding with ice particles during thermal motion can condense on them for the water vapor is oversaturated (Lübken 1999). Ignoring reverse process such as sublimation, the mass change rate for ice particles is  $\mu_{wd}m_w$ . The collision frequency  $\mu_{wd} = n_w\pi r_d^2 v_w$  based on the hard-sphere collision model (Lieberman and Lichtenberg 2005).  $m_w$ ,  $n_w$  and  $v_w$  are mass, number density and thermal velocity of water molecules, respectively.

The collision frequency between air molecules and ice particles in the neutral drag force term is (Schunk 1977)

$$\mu_{dn} = \frac{8}{3\sqrt{\pi}} \frac{n_n m_n}{m_d + m_n} \sqrt{\frac{2k_B T_g (m_d + m_n)}{m_d m_n}} \pi (r_d + r_n)^2 \quad (2)$$

where  $n_n$ ,  $m_n$ , and  $r_n$  are number density, mean molecule mass, and effective radius of neutral molecule, respectively.  $T_g$  is the gas temperature. The neutral molecule mass  $m_n$  is assumed as  $28.96m_u$ .  $m_u$  is the proton mass.

From Eq. (1) we can get the velocity of ice particles

$$\mathbf{u}_d = \mathbf{u} + \frac{m_d}{\mu_{dn} m_d + \mu_{wd} m_w} \mathbf{g} \quad (3)$$

With the facts that  $n_w \ll n_n$  (Seele and Hartogh 1999),  $m_w \ll m_d$ ,  $m_n \ll m_d$ ,  $r_n \ll r_d$  and  $v_n \sim v_w$ , and taking vertical up to be the positive direction, the velocity of ice particles is simplified as

$$u_d = u - g/\mu_{dn} \quad (4)$$

Ice particles are composed of condensation nuclei and attached ice. The mass of a single ice particle is

$$m_d = \frac{4}{3} \pi r_0^3 \rho_0 + \frac{4}{3} \pi (r_d^3 - r_0^3) \rho_d \quad (5)$$

where  $r_0$  and  $\rho_0$  are the initial radius and mass density of condensation nuclei, and  $\rho_d$  is the mass density of ice.

Based on the expressions of  $m_d$  and  $\mu_{dn}$ , the relationship between ice particle velocity and radius is

110 
$$u_d = u - \frac{g}{n_n m_n v_n} [\rho_d r_d + (\rho_0 - \rho_d) \frac{r_0^3}{r_d^2}] \quad (6)$$

At the upper and lower boundaries of study region, with  $r_d = r_0$  the initial velocity of condensation nuclei is

$$u_{d0} = u(1 - r_0/r_c) \quad (7)$$

$r_c$  is the critical radius

115 
$$r_c = n_n m_n v_n u / (g \rho_0) \quad (8)$$

When the radius of condensation nuclei  $r_0 > r_c$ , gravity is larger than the neutral drag force,  $v_{d0} < 0$ , and particles move downwards. Otherwise, particles move upwards.

Based on the relation of  $m_d$  with  $r_d$ , the change rate of ice particle radius is

$$\frac{dr_d}{dt} = \frac{1}{4} \frac{n_w m_w v_w}{\rho_d} = c \quad (9)$$

120 It is easy to see that the ice particle radius increases linearly with time

$$r_d = r_0 + ct \quad (10)$$

Then the particle trajectory can be obtained by the following integral

$$z - z_0 = \int_0^t u_d dt = c^{-1} \int_{r_0}^{r_d} u_d dr_d \quad (11)$$

125  $z_0$  is the reference height where condensation nuclei enter the studied region. It is set that  $z_0 = 0$  for the lower boundary and  $z_0 = h$  for the upper one, where  $h$  is the distance between the two boundaries.

We assume that the condensation nucleus radius ranging from  $r_{0\min}$  to  $r_{0\max}$  has a certain distribution function  $f(r_0)$ . The density of condensation nuclei with radius in a small scale  $r_0 \rightarrow r_0 + dr_0$  is  $dn(r_0) = f(r_0) dr_0$ , and their velocity is  $u_{d0}$ . When these particles arrive at height  $z$ , their radius increases to  $r_d(r_0, z)$ , the corresponding number density turns into  $dn(r_0, z)$ , and the velocity becomes  $u_d(r_0, z) = v_d[r_0, r_d(r_0, z)]$ . According to the particle-conservation law, we have

130

$$u_{d0} dn(r_0) = u_d(r_0, z) dn(r_0, z) \quad (12)$$

Then the number density of ice particles at height  $z$  can be obtained by

$$n_d(z) = \int dn(r_0, z) = \int_{r_{0\min}}^{r_{0\max}} \frac{u_{d0} f(r_0)}{u_d(r_0, z)} dr_0 \quad (13)$$

The average ice particle radius at height  $z$  is

$$\bar{r}_d(z) = \frac{\int r_d(z) dn(r_0, z)}{n_d(z)} \quad (14)$$

Through integrating all the condensation nucleus radii, stable distribution of  $n_d$  and  $r_d$  can be obtained. The particles keep entering and leaving the condensation region, but as long as the external environment does not change, the distribution of particle density and radius remains unchanged. Then the influence of these stable  $n_d$  and  $r_d$  profiles on electron and ion density is calculated.

140 Considering generation, recombination, and loss on particles, the continuity equation for ion density can be written as

$$\frac{\partial n_i}{\partial t} + \frac{\partial(n_i u_i)}{\partial z} = Q - \alpha n_i n_e - D^+ n_i \quad (15)$$

Ignoring gravity, the drift velocity of ions  $u_i$  is determined by

$$u_i = \frac{eE}{m_i \mu_{in}} - \frac{k_B T_g}{m_i \mu_{in}} \frac{1}{n_i} \frac{\partial n_i}{\partial z} \quad (16)$$

145 The electric field  $E$  is mainly determined by electron density gradient because the diffusion coefficient and mobility of electrons are much larger than that of ions:

$$E = -\frac{k_B T_g}{e} \frac{1}{n_e} \frac{\partial n_e}{\partial z} \quad (17)$$

In the typical PMSE layer, there are several kinds of ions carrying one unit positive charge:  $N_2^+$ ,  $O_2^+$ ,  $NO^+$  and  $H^+(H_2O)_n$ . According to Ref. (Reid 1990), the averaged ion parameters  $n_i$ ,  $m_i$ , and  $T_g$  are applied to describe the density, mass, and temperature of ions, respectively, and the averaged ion mass  $m_i$  is set as  $50m_u$ . According to Hill and Bowhill's theory (Hill and Bowhill 1977), the ion-neutral collision frequency is

$$\mu_{in} = 2.6 \times 10^{-15} n_n \left( 0.78 \frac{28}{M_i + 28} \sqrt{1.74 \frac{M_i + 28}{28 M_i}} + 0.21 \frac{32}{M_i + 32} \sqrt{1.57 \frac{M_i + 32}{32 M_i}} + 0.01 \frac{40}{M_i + 40} \sqrt{1.64 \frac{M_i + 40}{40 M_i}} \right) \quad (18)$$

where  $M_i = m_i/m_u$ .

155 The production rate for ions and electrons  $Q$  is chosen as  $3.6 \times 10^7 \text{ m}^{-3}\text{s}^{-1}$  and electron-ion recombination coefficient  $\alpha$  is set as  $10^{-12} \text{ m}^3\text{s}^{-1}$  (Lie - Svendsen, et al. 2003). Then the undisturbed density of ions and electrons  $n_0 = 6 \times 10^9 \text{ m}^{-3}$ . The loss coefficient of ions on ice particles  $D^+ = \sum n_q v_{i,q}$ , where  $n_q$  is the number density of the  $q$ -charged ice particles, and  $v_{i,q}$  represents the capture rate of ions by particles with  $q$  charges. According to the quantized stochastic charging model (Robertson and Sternovsky 2008):

$$v_{i,q \leq 0} = \pi r_d^2 c_i \left( 1 + C_q \sqrt{\frac{e^2}{16\epsilon_0 k_B T_g r_d}} + D_q \frac{e^2}{4\pi\epsilon_0 k_B T_g r_d} \right) \quad (19)$$

The particle radius  $r_d$  used here is the averaged radius  $\bar{r}_d$ , which is obtained according to Eq. (14). The ion thermal velocity  $c_i = (8k_B T_g / \pi m_i)$ .  $k_B$  is Boltzmann's constant and  $\epsilon_0$  is the permittivity of vacuum.  $C_q$  and  $D_q$  are given in Table 1 of Robertson and Sternovsky's work (Robertson and Sternovsky 2008).  
165 And the corresponding capture rates of electrons by particles (Robertson and Sternovsky 2008) are written as

$$v_{e,q \geq 0} = \pi r_d^2 c_e \left( 1 + C_q \sqrt{\frac{e^2}{16\epsilon_0 k_B T_g r_d}} + D_q \frac{e^2}{4\pi\epsilon_0 k_B T_g r_d} \right) \quad (20)$$

$$v_{e,q < 0} = \pi r_d^2 \gamma^2 c_e \exp \left[ -\frac{|q|e^2}{4\pi\epsilon_0 k_B T_g r_d \gamma} \left( 1 - \frac{1}{2\gamma(\gamma^2 - 1)|q|} \right) \right] \quad (21)$$

The thermal velocity of electrons  $c_e = (8k_B T_g / \pi m_e)$ , and the value of  $\gamma$  for each  $q$  is referred from Natanson's paper (Natanson 1960).  
170

Although the distribution of total particle density  $n_d = \sum n_q$  has reached stable state under the effects of gravity and neutral drag force, the number density of the  $q$ -charged ice particles  $n_q$  is dynamic in the charging process. The continuity equation for  $q$ -charged ice particles is

$$\frac{\partial n_q}{\partial t} = n_{q+1} v_{e,q+1} n_e + n_{q-1} v_{i,q-1} n_i - (n_q v_{e,q} n_e + n_q v_{i,q} n_i) \quad (22)$$

175 According to the growth and motion model, the maximum radius of ice particles involved in this study is about 11 nm (see below), which is similar to the ice particle radius (10 nm) used in the paper of Lie - Svendsen et al. (Lie - Svendsen, et al. 2003; Rapp and Lübken 2001). So based on their work, it is assumed that a single particle carries two negative charges at most, i.e.,  $q = -2, -1, 0$  and  $+1$  in this study.

180 According to the typical parameters in PMSE region(Rapp and Lübken 2001), the plasma Debye length  $\lambda_D$  is estimated to be about 9 mm, which is much smaller than the vertical spatial scale of PMSE layer. So the dusty plasma satisfies the quasi-neutral condition:

$$n_i + \sum_q qn_q = n_e \quad (23)$$

185 In subsequent calculations, parameters are taken in the atmospheric environment at altitude of 85 km. The number density of neutrals  $n_n = 2.3 \times 10^{20} \text{ m}^{-3}$ (Hill, et al. 1999), the number density of water vapor  $n_w = 2.5 \times 10^{14} \text{ m}^{-3}$ (Seele and Hartogh 1999), temperature  $T_g = 150 \text{ K}$ , the mass density of ice  $\rho_d = 1 \times 10^3 \text{ kg/m}^3$ , the velocity of neutral wind  $u = 3 \text{ cm/s}$ (Garcia and Solomon 1985), the mass density of condensation nucleus  $\rho_0 = 2.7 \times 10^3 \text{ kg/m}^3$ , and the growth rate of ice particles  $c \approx 7.8 \times 10^{-4} \text{ nm/s}$ . In this work, we only consider the growth and movement of condensation nucleus which fall from the upper boundary with initial radius  $r_0 > r_c$  and rise from lower boundary with  $r_0 \leq r_c$ .

### 190 3 Results and discussion

For simplicity, dimensionless parameters are used:

$$V_d = v_d/u, \quad \rho = \rho_d/\rho_0, \quad R_0 = r_0/r_c, \quad R_d = r_d/r_c \\ T = t/t_c, \quad Z = (z - z_0)/z_c$$

195 where  $t_c = r_c/c$ , which represents the time it takes for ice particle radius  $r_d$  growing to  $r_d + r_c$ , and  $z_c = ut_c$  is the distance that neutral wind moves during the time  $t_c$ . In this study  $r_c = 4.2 \text{ nm}$ ,  $t_c \approx 5385 \text{ s}$ , and  $z_c \approx 161 \text{ m}$ .

The expression for dimensionless ice particle velocity is

$$V_d = 1 - \rho R_d - (1 - \rho) \frac{R_0^3}{R_d^2} \quad (24)$$

The expressions for dimensionless position coordinate of particles based on  $T$  and  $R_d$  are

$$200 \quad Z(R_0, T) = T - \frac{1}{2} \rho T(T + 2R_0) - (1 - \rho) R_0^2 \frac{T}{T + R_0} \quad (25)$$

$$Z(R_0, R_d) = R_d - R_0 - \frac{1}{2} \rho (R_d^2 - R_0^2) + (1 - \rho) R_0^3 \left( \frac{1}{R_d} - \frac{1}{R_0} \right) \quad (26)$$

The relation between  $V_d$  and  $R_d$  is illustrated in Fig. 1(a), which shows that condensation nuclei with



initial radius  $R_0 \leq 1$  rise into the PMSE region through the lower boundary, while particles with  $R_0 > 1$  fall into the region from the upper boundary. At the beginning, the upward-moving particles accelerate and the downward ones decelerate due to  $\partial V_d / \partial R_d = 2 - 3\rho > 0$  when  $R_d = R_0$ . Later, with the increase of  $R_d$ ,  $\partial V_d / \partial R_d < 0$ , all particles will move with a downward acceleration, which makes them move downward eventually.

Figure 1(b) shows the movement curves of ice particles near the lower boundary. These particles, with an initial radius  $R_0 \leq 1$ , rise into the condensation layer. With the collection of ice, the grains become larger and heavier, which leads to the deceleration of the grains. And then, the grains will accelerate downward until they leave the condensation layer from the lower boundary. All particles rising from the lower boundary will retrace in the range of  $Z_m < Z < Z_M$ .

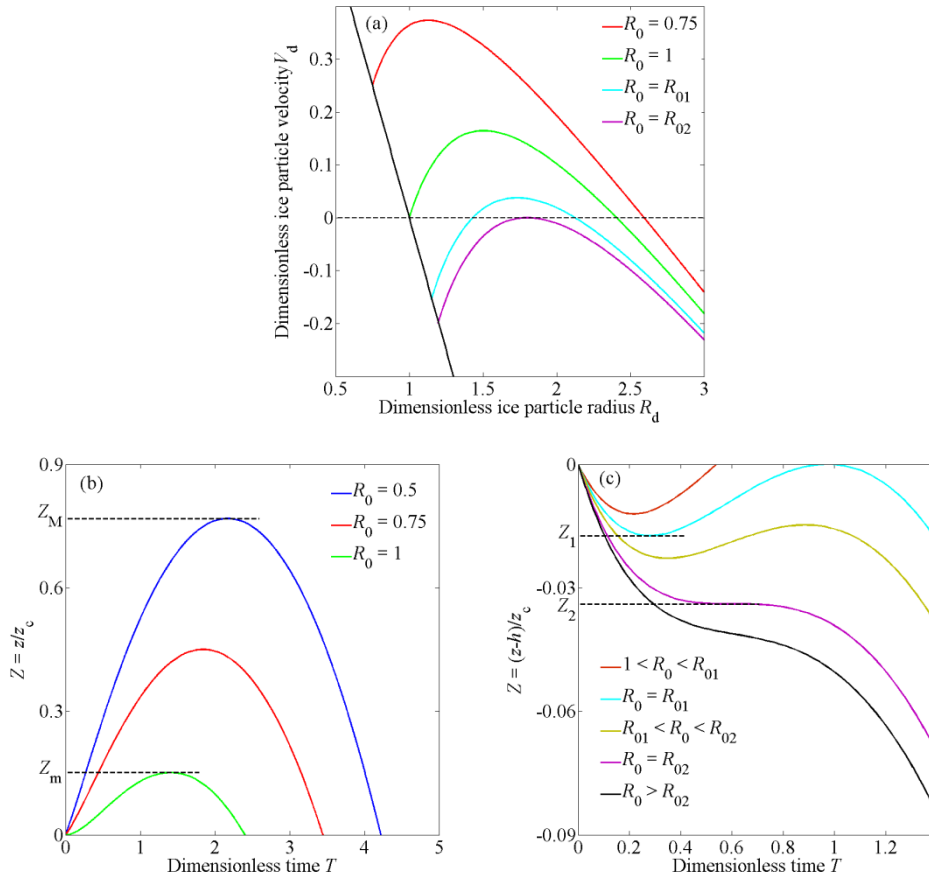


Figure 1 (a) The dependence of ice particle velocity on radius for different initial nuclei radii. The black solid line  $V_{d0} = 1 - R_0$  represents the distribution of initial particle velocity with respect to initial radius. (b) The movement curves of ice particles near the lower boundary. (c) The movement curves of ice particles near the upper boundary.  $Z_m$  is the

maximum height that particles with initial radius  $R_0 = 1$  can reach;  $Z_M$  is the maximum height that particles with initial radius  $R_0 = R_{0\min} = 0.5$  can reach. Based on above parameters,  $Z_m = 0.1512$  and  $Z_M = 0.7631$ .  $R_{01}$  and  $R_{02}$  are two critical values of condensation nucleus radius. For  $R_0 = R_{01}$  particles fall into the condensation layer, first retrace at height  $Z_1$ , and then retrace exactly at the upper boundary. When  $R_0 = R_{02}$ , the particles move down and reach the height  $Z_2$ , the velocity and acceleration are exactly zero, and then they continue to move down. According to above parameters,  $R_{01}$  and  $R_{02}$  are solved as 1.1519 and 1.19705, respectively.

Figure 1(c) shows the movement curves of ice particles near the upper boundary, which can be sorted by the value of  $R_0$ . For  $1 < R_0 < R_{01}$ , the neutral drag force increases faster than gravity as the particles fall. The particles decelerate to zero speed, retrace upward, and then leave the condensation layer from the upper boundary. For  $R_0 = R_{01}$ , the particles retrace at the height  $Z = Z_1$ . Then they arrive at  $Z = 0$  with exactly zero velocity, and the particles move back into the condensation layer again. For  $R_{01} < R_0 < R_{02}$ , the particles retrace upward in the range of  $Z_2 < Z < Z_1$  and move downward again before they reach the upper boundary. For  $R_0 = R_{02}$ , the particles decelerate downward until zero speed at  $Z = Z_2$ . Here, the acceleration happens to be zero. Then the gravity exceeds the drag force, and the particles accelerate downward. For  $R_0 > R_{02}$ , the particles keep going down after entering the condensation layer.

From Fig. 1, it is concluded that the particles with a certain range of initial radius will move up and down several times near the boundary, namely, ice particles will accumulate at that region and form some kind of small-scale density structure. The resulting number density and radius distribution of ice particles are

$$n_d(Z) = n_0 \int_{R_{0\min}}^{R_{0\max}} \frac{V_{d0} F(R_0)}{V_d[R_0, R_d(R_0, Z)]} dR_0 \quad (27)$$

$$\bar{R}_d(Z) = \frac{n_0}{n_d(Z)} \int_{R_{0\min}}^{R_{0\max}} \frac{R_d(Z) V_{d0} F(R_0)}{V_d[R_0, R_d(R_0, Z)]} dR_0 \quad (28)$$

where  $n_0$  is the density of condensation cores at the boundary, and is assumed as  $5 \times 10^8 \text{ m}^{-3}$  (Bardeen, et al. 2008). The normalized radius distribution function  $F(R_0)$  satisfies  $\int_{R_{0\min}}^{R_{0\max}} F(R_0) dR_0 = 1$ .

Firstly, the density and radius distribution of ice particles near the lower boundary are solved. It is shown in Fig. 1(b) that all ice particles with initial radius  $R_0 \leq 1$  will pass the range  $0 < Z < Z_m$  twice, so they contribute twice to the calculation of particle density. And in the height range  $Z_m < Z < Z_M$ , only the particles that reach the  $Z$  height can contribute to the density at  $Z$ . their density and mean radius near the lower boundary are shown below:

$$n_d(Z) = n_0 \int_{0.5}^{R_{0Z}} V_{d0} F(R_0) \left[ \frac{1}{V_{d1}(R_0, R_{d1})} + \frac{1}{|V_{d2}(R_0, R_{d2})|} \right] dR_0 \quad (29)$$

$$\bar{R}_d(Z) = \frac{n_0}{n_d(Z)} \int_{0.5}^{R_{0Z}} V_{d0} F(R_0) \left[ \frac{R_{d1}}{V_{d1}(R_0, R_{d1})} + \frac{R_{d2}}{|V_{d2}(R_0, R_{d2})|} \right] dR_0 \quad (30)$$

$R_{d1}$  and  $R_{d2}$  are particle radii when particles pass through the  $Z$  height;  $V_{d1}$  and  $V_{d2}$  are their corresponding velocities; the upper limit of integral  $R_{0Z}$  can be determined by

$$R_{0Z} = \begin{cases} 1 & \text{if } 0 < Z < Z_m \\ \text{solution of } (Z(R_{0Z}, R_d) = Z) & \text{if } Z_m < Z < Z_M \end{cases} \quad (31)$$

In this study, the radius distribution function of condensation cores is assumed as Gaussian distribution

$$F(R_0) = A \exp[-(R_0 - R_{00})^2 / \Delta^2] \quad (32)$$

where the center of the radius distribution function  $R_{00}$  is chosen as 0.8, the characteristic width  $\Delta = 0.01$ , and the corresponding normalized coefficient  $A = 56.4$ .

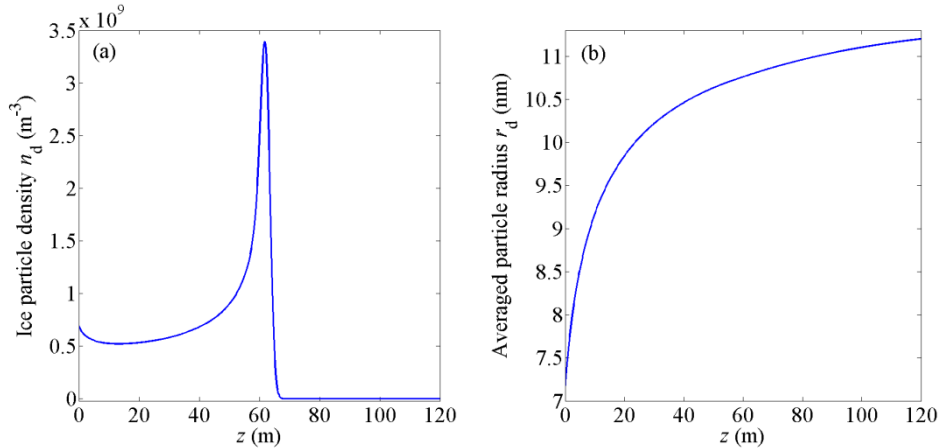
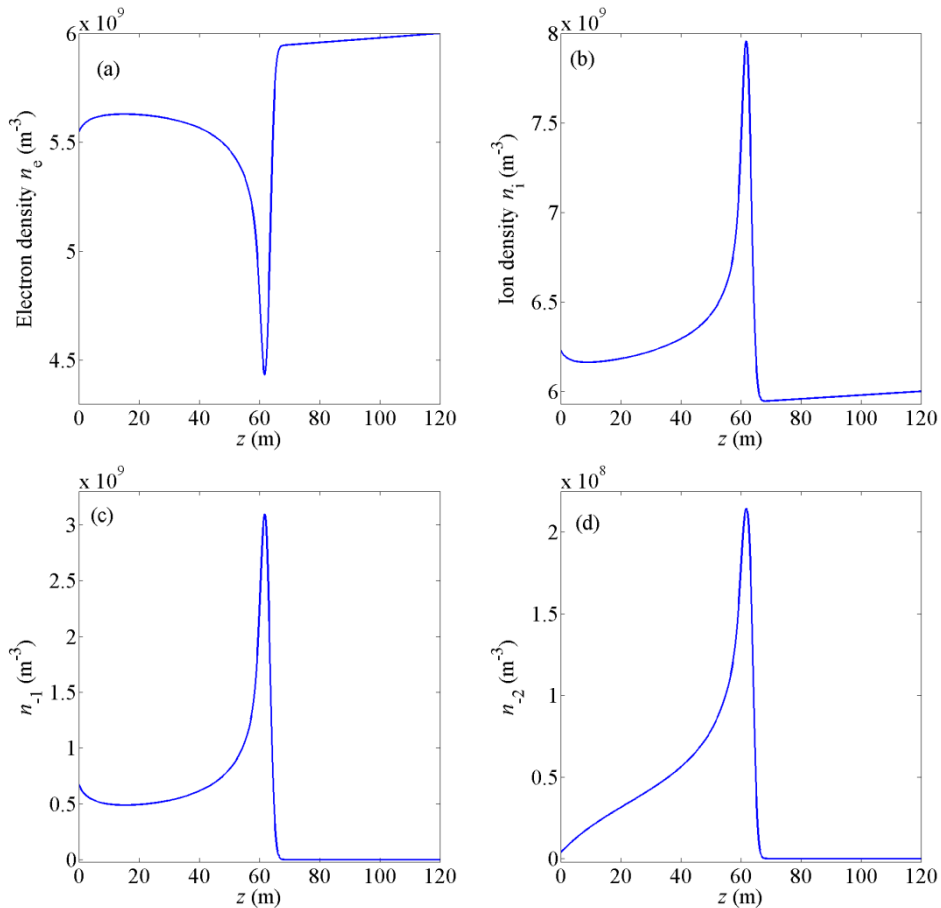


Figure 2 The distribution of (a) ice particle density and (b) mean particle radius near the lower boundary of condensation layer.

The obtained density and mean radius of ice particles near the lower boundary are present in Fig. 2(a) and 2(b) respectively. Figure 2(a) shows that a sharp peak appears in the density distribution of ice particles. The width at half maximum of the irregularity is about 5 meters, which is consistent with the assumed ice particle density structure scale in the theoretical work (Lie-Svendsen, et al. 2003; Rapp and

Lübken 2003) and observation by the sounding rocket flight ECT02 in July 1994 (Rapp and Lübken 2004). From Fig. 2(b), we can see that the average radius of ice particles increases from 7 nm to 11 nm with height.

265 With the obtained density and average radius of ice particles in Fig. 2(a) and Fig. 2(b), the density distribution of electrons, ions, and charged ice particles is calculated based on the charging model described by Eq. (15) ~ (23). At the initial moment of the charging model, all ice particles are assumed to be neutral to conduct the calculation more conveniently, since the final distributions of charge are independent on the initial ice particle charge state (Lie - Svendsen, et al. 2003). The timescale of  
 270 electron collected by negatively charged particles with a radius of 10 nm is about 700 s, which is the longest timescale in the charging process. And a quasi-steady state of charging can be obtained after this timescale. Therefore, the calculation is terminated after 1000 s and the results are illustrated in Fig. 3.



275 Figure 3 The number density distribution of (a) electrons  $n_e$ , (b) ions  $n_i$ , (c) particles carrying one negative charge  $n_{-1}$ ,

and (d) particles carrying two negative charges  $n_{-2}$  near the lower boundary of condensation layer at  $t = 1000$  s.

Figure 3(a) shows that electron density decreases sharply around  $z = 60$  m due to adsorption by particles. And the reduction of electron density  $\Delta n_e \approx (n_{-1} + 2n_{-2})/2$ , which is in line with the results under diffusion equilibrium approximations in (Lie - Svendsen, et al. 2003). Ion number density increases sharply around 60 m due to its movement under ambipolar electric field. The ambipolar diffusion process of electrons and ions has been described in detail in (Lie - Svendsen, et al. 2003). Electron density is anti-correlated to density irregularities of ions and charged ice particles due to attachment and diffusion processes. These anti-correlations are in agreement with rocket observations by the sounding rocket flight SCT-06 in August 1993 (Lie - Svendsen, et al. 2003) and the sounding rocket flight ECT02 in July 1994 (Rapp and Lübken 2004), respectively. It can be extracted from Fig. 3(c) and Fig. 3(d) that, for particles with radii ranging from 7 nm to 11 nm, the proportion of particles carrying one negative charge ranges from 97.5% to 85.1%, and that value for particles carrying two negative charges is 0.53% - 13.6%, which is consistent with observations by Havnes et al. (Havnes, et al. 1996) and numerical results by Rapp and Lübken (Rapp and Lübken 2001). The density of positively charged particles is less than  $1.1 \times 10^5 \text{ m}^{-3}$  and is insignificant in this study.

Next, the parameters of ice particles and plasma near the upper boundary are discussed based on the movement curves of ice particles near the upper boundary, which are shown below:

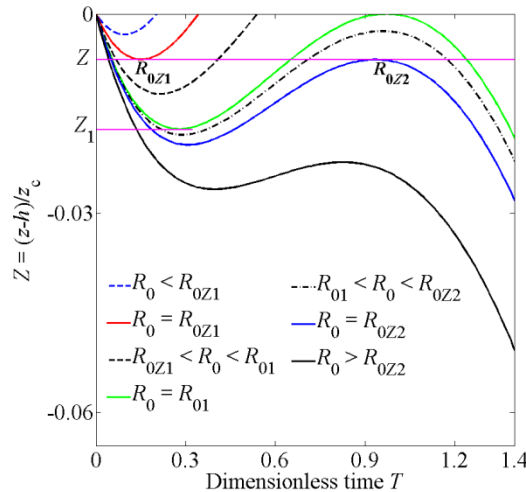


Figure 4 The movement curves of ice particles near the upper boundary. The particles with initial radius  $R_{0Z1}$  move upward after turning back at the  $Z$  height (the red line), and the particles with initial radius  $R_{0Z2}$  move downward after

turning back at  $Z$  (the blue line).

For  $Z_1 < Z < 0$ , two kinds of particles turn back at  $Z$ : particles with initial radius  $R_{0Z1}$  and  $R_{0Z2}$ . They go upward and downward separately as shown in Fig. 4. And the values of  $R_{0Z1}$  and  $R_{0Z2}$  are determined by equations  $V_d(R_{0Z}, R_d) = 0$  and  $Z(R_{0Z}, R_d) = Z$ . The contribution of ice particles to the density distribution near the upper boundary can be classified as follows:

(1)  $R_0 < R_{0Z1}$ : ice particles cannot reach  $Z$  and make no contributions to the number density.

(2)  $R_{0Z1} < R_0 < R_{01}$ : ice particles pass through  $Z$  twice and contribute to  $n_d(Z)$  twice. The radius of particles when passing through the  $Z$  height can be obtained as  $R_{d31}$  and  $R_{d32}$  based on Eq. (26). Meanwhile their corresponding velocities are calculated as  $V_{d31}$  and  $V_{d32}$  respectively based on Eq. (24).

(3)  $R_{01} < R_0 < R_{0Z2}$ : ice particles pass through  $Z$  three times. The corresponding radii and velocities at  $Z$  are defined as  $R_{d41}$ ,  $R_{d42}$ ,  $R_{d43}$ ;  $V_{d41}$ ,  $V_{d42}$ ,  $V_{d43}$ .

(4)  $R_0 > R_{0Z2}$ : ice particles pass through  $Z$  only once and their radius and velocity are  $R_{d5}$  and  $V_{d5}$ , respectively.

Substituting these parameters into Eq. (27) and (28), the density and mean radius of ice particles in the range of  $Z_1 < Z < 0$  are deduced as

$$n_d(Z) = n_0 \int_{R_{0Z1}}^{R_{01}} V_{d0} F(R_0) \left[ \frac{1}{|V_{d31}(R_0, R_{d31})|} + \frac{1}{V_{d32}(R_0, R_{d32})} \right] dR_0 \\ + n_0 \int_{R_{01}}^{R_{0Z2}} V_{d0} F(R_0) \left[ \frac{1}{|V_{d41}(R_0, R_{d41})|} + \frac{1}{V_{d42}(R_0, R_{d42})} + \frac{1}{|V_{d43}(R_0, R_{d43})|} \right] dR_0 \\ + n_0 \int_{R_{0Z2}}^{R_{0\max}} \frac{V_{d0} F(R_0)}{|V_{d5}(R_0, R_{d5})|} dR_0 \quad (33)$$

$$\bar{R}_d(Z) = \frac{n_0}{n_d(Z)} \int_{R_{0Z1}}^{R_{01}} V_{d0} F(R_0) \left[ \frac{R_{d31}}{|V_{d31}(R_0, R_{d31})|} + \frac{R_{d32}}{V_{d32}(R_0, R_{d32})} \right] dR_0 \\ + \frac{n_0}{n_d(Z)} \int_{R_{01}}^{R_{0Z2}} V_{d0} F(R_0) \left[ \frac{R_{d41}}{|V_{d41}(R_0, R_{d41})|} + \frac{R_{d42}}{V_{d42}(R_0, R_{d42})} + \frac{R_{d43}}{|V_{d43}(R_0, R_{d43})|} \right] dR_0 \\ + \frac{n_0}{n_d(Z)} \int_{R_{0Z2}}^{R_{0\max}} \frac{R_{d5} V_{d0} F(R_0)}{|V_{d5}(R_0, R_{d5})|} dR_0 \quad (34)$$

where the radius distribution function of condensation cores  $F(R_0)$  are set to satisfy the Gaussian distribution with the distribution function center  $R_{00} = 1.08$ , the characteristic width  $\Delta = 0.01$ , and the corresponding normalized coefficient  $A = 56.4$ .

The ice particle density in the range of  $Z < Z_1$  is close to zero, since only particles with initial radius  $R_0 \geq R_{01}$  can arrive at the range and the number of particles in this radius range is very few based on the parameters of  $F(R_0)$  set above.

At the upper boundary, the number density of condensation cores  $n_0$  is set as  $5 \times 10^8 \text{ m}^{-3}$ ; the maximum radius of condensation cores  $R_{0\text{max}} = 1.3$ . The number density and mean radius of ice particles are obtained from Eq. (33) and (34). Then the density distribution of electrons, ions, and charged ice particles is calculated further based on the charging model.

Figure 5(a) shows that there is a meter scale structure in the distribution of ice particle density, which is consistent with the assumed ice particle density structure scale in previous theoretical work (Lie - Svendsen, et al. 2003; Rapp and Lübken 2003) and rocket observations (Rapp and Lübken 2004). The average radius of ice particles is slightly larger than 5 nm (shown in Fig. 5(b)).

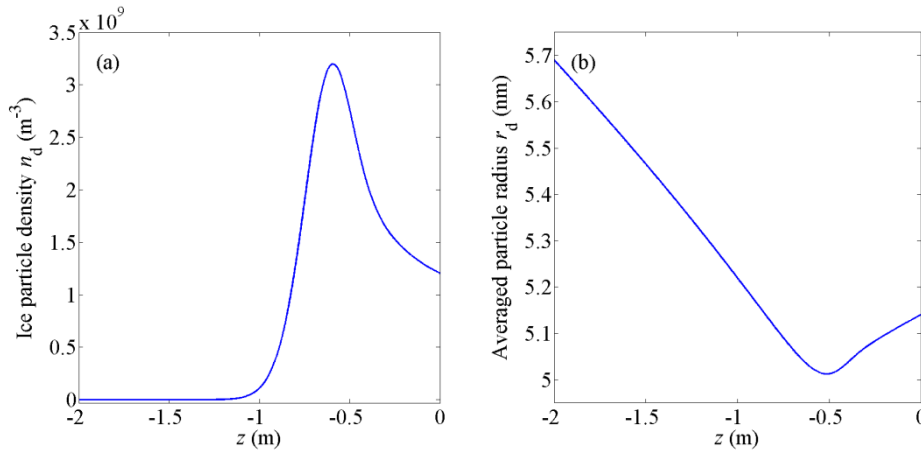
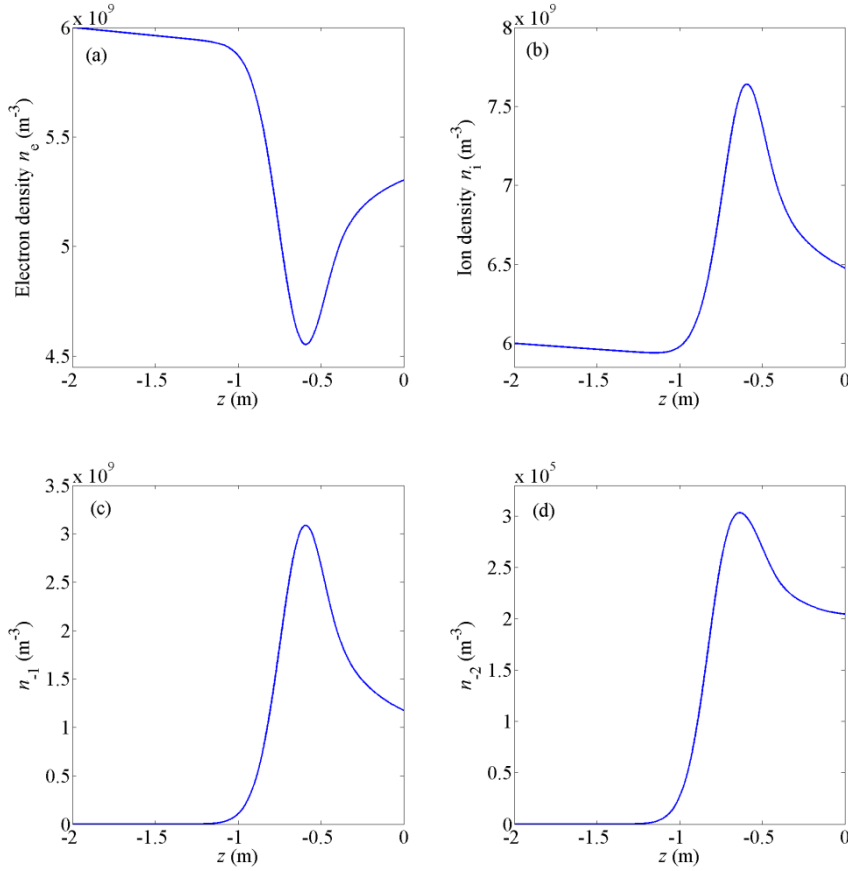


Figure 5 The distribution of (a) ice particle density and (b) mean particle radius near the upper boundary of condensation layer.

Figure 6(a) shows that, compared with ice particle density, there is a similar but anti-correlated structure in electron density profile because of the adsorption of electrons by particles. Due to ambipolar diffusion, ion density increases in the perturbed region. The reduction of electron density  $\Delta n_e$  and the increment of ion density  $\Delta n_i$  meet with the results under diffusion equilibrium approximations:  $\Delta n_e \approx \Delta n_i \approx (n_{-1} + 2n_{-2})/2$  (Lie - Svendsen, et al. 2003). From Fig. 6(c) and Fig. 6(d) we can see that, 97% of the particles carry one negative charge, and particles carrying two negative charges are very few. This is reasonable for particles with radius slightly larger than 5 nanometers.



340 Figure 6 The number density distribution of (a) electrons, (b) ions, (c) particles carrying one negative charge, and (d) particles carrying two negative charges near the upper boundary of condensation layer at  $t = 1000$  s.

#### 4 Conclusions

In summary, a possible formation mechanism of small scale ice particle density irregularities in PMSE region is presented, and the influence of these irregularities on plasma density profile is studied.

345 Firstly, a growth and motion model of ice particles is developed based on the adsorption of water vapor by particles and dynamic equation for variable mass object. Then the density profile of ice particles with height is investigated according to the conservation of particle number. Finally, on the basis of quasi-neutrality and the quantized stochastic charging model, the corresponding density distribution of electrons, ions, and charged ice particles is obtained. In the calculation, the parameters are chosen



350 corresponding to an altitude of 85 km, where PMSEs are often detected.

The results show that the ice particle radius increases linearly with time. But, there is a complex relation between the velocity and radius of particles due to the different mass densities of condensation nuclei and absorbed ice. And for a certain radius of the condensation nucleus, particles can bounce and gather locally. When the radius distribution function of condensation nucleus is Gaussian, stable  
355 small-scale ice particle density structures can be obtained based on the growth and motion model. Because of the plasma attachment by ice particles and plasma diffusion, electron density decreases in the disturbed region, while ion density increases in the region, i.e., the electron density is anti-correlated to charged ice particle density and ion density, which is in consistent with most rocket observations. Furthermore, the reduction of electron density and the increment of ion density are about half the charge  
360 number density of ice particles, which is in line with the results under diffusion equilibrium approximations.

### **Acknowledgements**

The research has been financially supported by the National Natural Science Foundation of China under Grant Nos. 11775062 and 61601419.

### 365 **REFERENCE**

- Bardeen C., Toon O., Jensen E., etc.: Numerical simulations of the three - dimensional distribution of meteoric dust in the mesosphere and upper stratosphere, *Journal of Geophysical Research: Atmospheres*, 113, D17202, 2008.
- Chen C., Scales W.: Electron temperature enhancement effects on plasma irregularities associated with  
370 charged dust in the Earth's mesosphere, *Journal of Geophysical Research: Space Physics*, 110, 2005.
- Garcia R. R., Solomon S.: The effect of breaking gravity waves on the dynamics and chemical composition of the mesosphere and lower thermosphere, *Journal of Geophysical Research: Atmospheres*, 90, 3850-3868, 1985.
- 375 Havnes O., Trøim J., Blix T., etc.: First detection of charged dust particles in the Earth's mesosphere, *Journal of Geophysical Research: Space Physics*, 101, 10839-10847, 1996.
- Hill R., Bowhill S.: Collision frequencies for use in the continuum momentum equations applied to the lower ionosphere, *Journal of Atmospheric and Terrestrial Physics*, 39, 803-811, 1977.
- Hill R., Gibson-Wilde D., Werne J., etc.: Turbulence-induced fluctuations in ionization and application  
380 to PMSE, *Earth, planets and space*, 51, 499-513, 1999.

- Jensen E., Thomas G. E.: A growth - sedimentation model of polar mesospheric clouds: Comparison with SME measurements, *Journal of Geophysical Research: Atmospheres*, 93, 2461-2473, 1988.
- Körner U., Sonnemann G.: Global three - dimensional modeling of the water vapor concentration of the mesosphere - mesopause region and implications with respect to the noctilucent cloud region, *Journal of Geophysical Research: Atmospheres*, 106, 9639-9651, 2001.
- 385 Lübken F. J.: Thermal structure of the Arctic summer mesosphere, *Journal of Geophysical Research: Atmospheres*, 104, 9135-9149, 1999.
- Lübken F. J., Rapp M., Blix T., etc.: Microphysical and turbulent measurements of the Schmidt number in the vicinity of polar mesosphere summer echoes, *Geophysical Research Letters*, 25, 893-896, 1998.
- 390 Lie - Svendsen Ø., Blix T., Hoppe U. P., etc.: Modeling the plasma response to small - scale aerosol particle perturbations in the mesopause region, *Journal of Geophysical Research: Atmospheres*, 108, 8442, 2003.
- Lieberman M. A., Lichtenberg A. J.: *Principles of plasma discharges and materials processing*, John Wiley & Sons, 2005.
- 395 Mahmoudian A., Scales W.: On the signature of positively charged dust particles on plasma irregularities in the mesosphere, *Journal of Atmospheric and Solar-Terrestrial Physics*, 104, 260-269, 2013.
- Natanson G.: On the theory of the charging of amicroscopic aerosol particles as a result of capture of gas ions, *Sov. Phys. Tech. Phys.*, 30, 573-588, 1960.
- 400 Pfaff R., Holzworth R., Goldberg R., etc.: Rocket probe observations of electric field irregularities in the polar summer mesosphere, *Geophysical research letters*, 28, 1431-1434, 2001.
- Röttger J., La Hoz C., Kelley M. C., etc.: The structure and dynamics of polar mesosphere summer echoes observed with the EISCAT 224 MHz radar, *Geophysical research letters*, 15, 1353-1356, 1988.
- 405 Röttger J., Rietveld M., La Hoz C., etc.: Polar mesosphere summer echoes observed with the EISCAT 933 - MHz radar and the CUPRI 46.9 - MHz radar, their similarity to 224 - MHz radar echoes, and their relation to turbulence and electron density profiles, *Radio Science*, 25, 671-687, 1990.
- Rapp M., Lübken F.-J.: Modelling of particle charging in the polar summer mesosphere: Part 1—General results, *Journal of Atmospheric and Solar-Terrestrial Physics*, 63, 759-770, 2001.
- 410 Rapp M., Lübken F.-J.: Polar mesosphere summer echoes (PMSE): Review of observations and current understanding, *Atmospheric Chemistry and Physics*, 4, 2601-2633, 2004.
- Rapp M., Lübken F. J.: On the nature of PMSE: Electron diffusion in the vicinity of charged particles revisited, *Journal of Geophysical Research: Atmospheres*, 108, 8437, 2003.
- 415 Reid G. C.: Ice particles and electron “bite - outs” at the summer polar mesopause, *Journal of Geophysical Research: Atmospheres*, 95, 13891-13896, 1990.
- Robertson S., Sternovsky Z.: Effect of the induced-dipole force on charging rates of aerosol particles,

Physics of Plasmas, 15, 040702, 2008.

420 Scales W., Ganguli G.: Investigation of plasma irregularity sources associated with charged dust in the Earth's mesosphere, Advances in Space Research, 34, 2402-2408, 2004.

Schunk R.: Mathematical structure of transport equations for multispecies flows, Reviews of Geophysics, 15, 429-445, 1977.

425 Seele C., Hartogh P.: Water vapor of the polar middle atmosphere: Annual variation and summer mesosphere conditions as observed by ground - based microwave spectroscopy, Geophysical Research Letters, 26, 1517-1520, 1999.